

# Structural Signatures of Vitrification in Hard Core Fluids

Sanat K. Kumar\*, Shekhar Garde

*Department of Chemical Engineering,  
Rensselaer Polytechnic Institute, Troy, NY*

Jack F. Douglas, Francis W. Starr

*Polymers Division and Center for Theoretical and Computational Materials Science,  
National Institutes of Standards and Technology, Gaithersburg, MD*

## Abstract

Computer simulations of hard spheres and disks are used to estimate the most probable cavity size,  $\xi_{\text{cavity}}$ , and a “rattle” size,  $\xi_{\text{rattle}}$ , over which a particle can translate holding all other particles fixed. Both of these measures of free volume appear to extrapolate to zero at the random close packed density,  $\rho_{\text{rcp}}$ , close to the density where extrapolations of the viscosity diverge. We also identify the onset of caging as the density at which cavities cluster. These results suggest that vitrification in hard core fluids can be viewed as a geometrical phenomenon, and that *local* free volume measures can identify the location of the onset of liquid-like dynamics, the complex dynamics of caged liquids, and vitrification.

---

\* E-mail:kumar@rpi.edu

Ensembles of hard spheres have long been utilized as prototypical models for liquids and solids. Since these systems can be defined purely by geometry, it seems reasonable to understand them in terms of void or “free” volume. Thus, a class of models, termed “free volume” models have been very popular in describing the transition of hard core fluids from the gas to the liquid state, from the liquid to the crystal and from the liquid to the glassy state [1, 2, 3, 4, 5]. In spite of the popularity of these ideas, the molecular connection between “free volume” and dynamic transitions in these fluids remains unclear [6]. Previous molecular dynamics simulations [7, 8, 9] have identified many dynamic signatures of the vitrification of hard core fluids and it is our goal to enunciate any underlying structural indicators.

We simulate hard spheres and hard disks using the Monte Carlo method and periodic boundary conditions. The lateral size of the system,  $L$ , and the number of particles,  $N$ , are held fixed in each simulation. We used  $L=100$  in two dimensions ( $D=2$ ) and up to  $L=60$  for  $D=3$ . Density, or equivalently volume fraction, is defined as  $\rho \equiv \frac{\pi\sigma^2 N}{4L^2}$  in  $D=2$  and  $\rho \equiv \frac{\pi\sigma^3 N}{6L^3}$  in  $D=3$  where  $\sigma$  is the particle diameter. (We report lengths in units of  $\sigma$ .) We generate random initial configurations, and thus some particle overlap was initially unavoidable at the highest densities. Equilibration was monitored by comparing various system properties, including the pressure and the chemical potential, to literature estimates (for example [10]). We also confirmed that system did not “age” as a function of time over the course of the simulations ( $10^6$  attempted moves/particle at all densities).

Representative particle configurations for relatively low ( $\rho=0.40$ ) and high density ( $\rho=0.53$ ) hard disc ( $D=2$ ) fluids are shown in Fig. 1. Note that although the disks are themselves of diameter 1, we have drawn regions of exclusion of diameter 2 in this figure. Thus, the unshaded areas correspond to regions where centers of new particles can be accommodated in the fluid without overlap. We observe that the “voids” in this figure become smaller and sparser as the  $\rho$  increases, and it is this effect we quantify in this paper.

We evaluate two characteristic structural size scales using algorithms based on particle insertions [11, 12]. Following Ref. [12], “cavity” size distributions are defined by randomly selecting points in space and determining the size of the largest spherical cavity that can be inserted about them. This definition of a “cavity” is notably different from that employed in refs. [13, 14]. The distribution function for these maximal spheres displays a single peak, which is the most probable cavity size,  $\xi_{\text{cavity}}$ . We expect  $\xi_{\text{cavity}}$  to be related to

characteristic cavity sizes measured by positron annihilation lifetime spectroscopy, but the precise relationship has not been conclusively demonstrated. We find that  $\xi_{\text{cavity}}$  varies linearly with  $1/\beta\mu$ . Since both  $\beta\mu$  and the viscosity of these fluids are expected to diverge near the random closed pack limit [10, 15, 16, 17, 18], a phenomenological connection between system dynamics and the presence of cavities is implied. *We note that, although the most probable cavity size is expected to go to zero in this limit, cavities are still expected to exist beyond this point.*

Another useful measure of free volume is the “rattle volume” which corresponds to the volume explored by a particle given the constraints of surrounding particles [4, 7, 8]. Rattle size is evaluated in two equivalent ways. We consider the equilibrium distribution of acceptable displacements,  $p_{\text{disp}}(r)$ , made by randomly selected particles while holding all other particles fixed (see Fig. 1b). The maximum test displacement size is the box size so that all possible displacements are sampled. Alternatively, we can obtain the same results by considering successful insertions of pairs of spheres of size unity into the fluid without overlap, and constructing a probability distribution function for their separations. Notably,  $p_{\text{disp}}(r)$  has a peak at small  $r$  values for  $\rho \gtrsim 0.25$  in  $D=3$ , and for  $\rho \gtrsim 0.35$  in  $D=2$  (see Fig. 1b inset). Since the chosen particle is hindered by surrounding particles for distances beyond the peak, we identify the peak as the most probable rattle size,  $\xi_{\text{rattle}}$ . Past work [4] suggests that this rattle size is closely related to the Debye-Waller factor derived from dynamic scattering experiments.

The fact that there is no peak in  $p_{\text{disp}}(r)$  for  $\rho \leq 0.25$  ( $D=3$ ) and  $\rho \leq 0.35$  ( $D=2$ ), implies that there is no well-defined rattle volume in this density range, i.e., particles can freely move over the whole volume, as expected for a gas. For higher densities, however, our results suggest that rattle sizes are no longer “extensive” (i.e., scales with the system size), suggesting that holes are localized [see Fig. 1]. This is consistent with the fact that  $\rho \approx 0.26$  has previously been assigned as the onset of the “fluid” region for hard sphere dynamics ( $D=3$ ), where the free volume no longer percolates [5]. Hence,  $\xi_{\text{rattle}}$  identifies the region where hard fluid transport becomes liquid-like. Note that this density is much less than the density at the onset of “caging” in the dynamics, i.e.,  $\rho = 0.53$  for  $D=3$ , as we shall discuss below [19]. To further test the utility of  $\xi_{\text{rattle}}$ , we consider the Lindemann criterion as applied to an amorphous phase [20]. This criterion requires that the ratio of the mean rattle distance to the interparticle distance be  $\approx 0.1$ - $0.15$  at the transition density. Specifically, for

both spheres and disks we find that  $\xi_{\text{rattle}} \rho^{1/D} \approx 0.08 \pm 0.02$  at the crystallization density, consistent with this generalized Lindemann criterion. These two results support the utility of these free volume ideas.

Fig. 2 shows our results for  $\xi_{\text{rattle}}$  for a range of  $\rho$  in both  $D=3$  and  $D=2$ . We also plot the experimental cage sizes obtained from the dynamics of hard spheres to demonstrate the connection between equilibrium properties and dynamics in these situations [19, 21]. As a first step towards understanding the density dependence of  $\xi_{\text{rattle}}$ , we note that in a simple “cell” model of a dense homogeneous fluid, the cage size,  $\xi$ , is comparable to the average interparticle distance, so that  $\xi$  scales as  $\rho^{-1/D}$  at low densities and goes to 0 in the limit of close packing. In Fig. 2 we compare  $\xi_{\text{rattle}}$  to the interpolation formula,  $\xi \propto \left[ \left( \frac{\rho_{\text{rcp}}}{\rho} \right)^{1/D} - 1 \right]$  connecting these two limits. We employed this formula with proportionality constants  $\alpha=0.87$  ( $D=2$ ), and  $\alpha=1.4$  ( $D=3$ ) and literature values of  $\rho_{\text{rcp}}=0.83$  ( $D=2$ ) and  $0.644$  ( $D=3$ ), respectively. These results are consistent with the notion that this molecular measure of free volume vanishes in the limit of random closed packing. Alternate forms often employed for studying dynamic properties, such as  $\xi_{\text{rattle}} \sim (\rho_{\text{rcp}}/\rho - 1)^\gamma$  or  $\xi_{\text{rattle}} \sim (1 - \rho/\rho_{\text{rcp}})^\gamma$ , also provide adequate fits to these data, reiterating this fact. The cavity size,  $\xi_{\text{cavity}}$ , also follows the same density dependence with  $\alpha=0.345$  ( $D=3$ ) [Fig. 3]. However, for  $D=2$  we had to fit both  $\alpha=0.038$  and  $\rho_{\text{rcp}}=0.79$  to obtain good agreement with simulations, due to the large error bars associated with this small quantity. Note that the number of data points for  $\xi_{\text{cavity}}$  are typically different from  $\xi_{\text{rattle}}$  due to sampling issues that make the evaluation of  $\xi_{\text{rattle}}$  difficult at high densities.

These plots exhibit the usual problem that the value of  $\rho$  where  $\xi_{\text{rattle}}$  and  $\xi_{\text{cavity}} \rightarrow 0$  depends sensitively on how we extrapolate to higher densities. To illustrate this point, we note that both  $\xi_{\text{rattle}}$  and  $\xi_{\text{cavity}}$  vary nearly linearly with  $\rho$  for  $0.3 \leq \rho < 0.45$  for  $D=3$ , and for  $0.5 \leq \rho < 0.65$  for  $D=2$ . Curiously, linear extrapolations of the low density  $\xi_{\text{rattle}}$  and  $\xi_{\text{cavity}}$  data to zero yield  $\rho_G=0.56 \pm 0.03$  for  $D=3$  and  $\rho_G=0.74 \pm 0.05$  for  $D=2$  [22]. The density estimate in  $D=3$  closely matches the reported experimental glass transition density,  $\rho_G \approx 0.56 - 0.58$  presented by [9, 16, 23], where diffusion coefficient data were extrapolated to zero over the restricted range  $\rho \leq 0.52$ . The significance of this coincidence is unclear, since experiments and simulations where higher density data are considered (e.g., [15, 16, 17, 18]) suggest that the viscosity does not diverge at  $\rho_G$ , but rather at a density close to  $\rho_{\text{rcp}}$ . Similarly, we find that a plot of the logarithm of literature diffusivity data [16] varies linearly

with  $\xi_{\text{rattle}}^{-2}$ , in agreement with the notion that random closed packing is close to the point where the system “vitrifies” [4]. However, we note that the determination of the exact density at which the viscosity diverges is somewhat uncertain due to the inherent errors in the high density data and the extrapolation process. For two dimensional disks, the “glass transition” density is harder to locate since most simulations introduce polydispersity to prevent crystallization. For polydisperse disks there is the estimate  $\rho_G \approx 0.8$  [24, 25], but this number is probably larger than for the monodisperse limit. Our  $\rho_G$  estimate thus does match the experimental estimates obtained from extrapolation of low density data.

Above we noted that visual examination of fluid configurations suggest that small, complex shaped cavities become increasingly separated with increasing  $\rho$  (Fig. 1). We next define a scale relevant to the typical separation of the “void clusters”. We expect that spatial correlations associated with these void structures may have some relation to dynamic heterogeneities in the dense fluid regime [24, 26, 27], but the exact relationship is currently unclear. Specifically, we consider the distance away from a given insertion point that we must go such that the probability of insertions in a spherical (circular in  $D=2$ ) shell is larger than the peak probability of insertion, located in the immediate vicinity ( $r < 1$ ) of the first insertion point. For example, Fig. 1b shows that this “crossover” scale,  $\xi_{\text{cross}}$ , at which insertions become more probable than in the immediate neighborhood occurs at  $\approx 8$  for  $\rho = 0.4$ . For randomly chosen insertions points, we expect the scale for successive insertions to be  $\xi_{\text{rand}} = (1/p_{\text{ins}})^{1/D}$ , which naturally increases for increased  $\rho$ . [ $p_{\text{ins}}$  is the insertion probability for a sphere into a snapshot of the fluid.] It is natural to then consider the role of correlations by comparing the behavior of  $\xi_{\text{cross}}$  and  $\xi_{\text{ran}}$ . Fig. 4 shows both  $\xi_{\text{cross}}$  and  $\xi_{\text{ran}}$  as a function of  $\rho$ . At small  $\rho$ ,  $\xi_{\text{cross}} < \xi_{\text{ran}}$ , apparently reflecting the tendency of particles to be clustered in the fluid (Fig. 1). There is a characteristic  $\rho$  where  $\xi_{\text{cross}}$  first exceeds  $\xi_{\text{ran}}$ , and under these conditions we suggest that it is the holes that now cluster. Notably, the density where  $\xi_{\text{cross}} = \xi_{\text{ran}}$  corresponds to the density identified as the onset of “caged” dynamics in both  $D=2$  ( $\rho \approx 0.48$ ) [28] and  $D=3$  ( $\rho \approx 0.53$ ) [19, 23]. Hence, we tentatively identify the point where the holes cluster as the onset of complex, structured fluid behavior, and possibly a structural indicator of the onset of dynamical heterogeneity.

It is useful to contrast our work to Ref. [4], which has shown that the rattle volume vanishes in the vicinity of the Vogel temperature for Lennard-Jones particles. For hard spheres, our results suggest that random close packing plays the role of the “Vogel” point, i.e., the

density where the viscosity diverges and the free volume extrapolates to zero. Additionally, an alternate measure of the range of structure provides an estimate of the onset of caging.

We acknowledge the National Science Foundation , Division of Materials Research for funding, and Ralph Colby, Pablo Debenedetti and Robin Speedy for useful discussions.

- 
- [1] A. K. Doolittle, *J. Appl. Phys.* **22**, 1031 (1951).
- [2] M. H. Cohen and D. Turnbull, *J. Chem. Phys.* **31**, 1164 (1959).
- [3] M. H. Cohen and G. S. Grest, *Phys. Rev. B* **20**, 1077 (1979).
- [4] F. W. Starr, S. Sastry, J. F. Douglas, and S. C. Glotzer, *Phys. Rev. Lett.* **89**, 125501 (2002).
- [5] P. V. Giaquinta and G. Giunta, *Physica A* **187**, 145 (1992).
- [6] J. L. Finney and J. Wallace, *J. Non-Crystl. Solids* **43**, 165 (1981).
- [7] W. G. Hoover, W. T. Ashurst, and R. Grover, *J. Chem. Phys.* pp. 1259–1262 (1972).
- [8] D. Henderson, K.-Y. Chan, and L. Degreve, *J. Chem. Phys.* **101**, 6975 (1994).
- [9] B. J. Alder, D. M. Gass, and T. E. Wainwright, *J. Chem. Phys.* **53**, 3813 (1970).
- [10] M. D. Rintoul and S. Torquato, *Phys. Rev. Lett.* **77**, 4198 (1996).
- [11] H. Reiss and A. D. Hammerich, *J. Phys. Chem.* **90**, 6252 (1986).
- [12] A. Pohorille and L. R. Pratt, *J. Am. Chem. Soc.* **112**, 5066 (1990).
- [13] R. J. Speedy and H. Reiss, *Mol. Phys.* **72**, 999 (1991).
- [14] S. Sastry, T. M. Truskett, P. G. Debenedetti, S. Torquato, and F. H. Stillinger, *Mol. Phys.* **95**, 289 (1998).
- [15] Z. Cheng, J. Zhu, P. M. Chaikin, S.-E. Phan, and W. B. Russel, *Phys. Rev. E* **65**, 041405 (2002).
- [16] L. V. Woodcock and C. A. Angell, *Phys. Rev. Lett.* **47**, 1129 (1981).
- [17] E. R. Weeks, J. C. Crocker, A. C. Levitt, A. Schofield, and D. A. Weitz, *Science* **287**, 627 (2000).
- [18] J. Zhu, M. Li, R. Rogers, W. Meyer, R. H. Ottewill, S. S. S. Crew, W. B. Russel, and P. M. Chaikin, *Nature* **387**, 883 (1997).
- [19] B. Doliwa and A. Heuer, *Phys. Rev. Lett.* **80**, 4915 (1998).
- [20] X. Xia and P. G. Wolynes, *Proc. Nat. Acad. Sci.* **97**, 2990 (2000).
- [21] E. R. Weeks and D. A. Weitz, *Phys. Rev. Lett.* **89**, 095704 (2002).
- [22] R. J. Speedy, *J. Phys. Condens. Matt.* **10**, 4185 (1998).
- [23] A. Kasper, E. Bartsch, and H. Sillescu, *Langmuir* **14**, 5004 (1998).
- [24] B. Doliwa and A. Heuer, *Phys. Rev. E* **61**, 6898 (2000).
- [25] L. Santen and W. Krauth, *Nature* **405**, 550 (2000).

- [26] T. Schröder, S. Sastry, J. C. Dyre, and S. C. Glotzer, *J. Chem. Phys.* **112**, 9834 (2000).
- [27] C. Bennemann, C. Donati, J. Baschnagel, and S. C. Glotzer, *Nature* **399**, 246 (1999).
- [28] A. H. Marcus, J. Schofield, and S. A. Rice, *Phys. Rev. E* **60**, 5725 (1999).



## Figure Captions

1. (a) Typical snapshots of the  $D=2$  fluid. We show small portions of the simulation cell for ease of visualization, and the circles drawn have a radius of 1. Thus, the white spaces in these figures represent areas where centers of additional disks can be placed without overlap. The left snapshot is for a density  $\rho=0.4$ , while the right picture is at  $\rho=0.53$ . (b) Main plot:  $p_{\text{disp}}(r)/4\pi$  as a function of  $r$  for the three dimensional hard sphere fluid at  $\rho=0.4$ . The two arrows represent characteristic sizes: the one closest to the origin is  $\xi_{\text{rattle}}$ , while the other distance is  $\xi_{\text{cross}}$ . The  $p_{\text{disp}}(r)$  is used to generate  $y(r) \equiv \frac{p_{\text{disp}}(r)\Gamma(D/2)}{2\pi^{D/2}r^{D-1}}$ , where  $\Gamma(x)$  is the gamma function, and  $2\pi^{D/2}r^{D-1}/\Gamma(r)dr$  is the volume of a D-dimensional hypersphere shell of radius  $r$  and thickness  $dr$ . The distance and density dependence of  $y(r)$  for  $\rho \leq 0.495$  for  $D=3$  are consistent with past results [8]. Inset: Plot of  $p_{\text{disp}}(r)/4\pi$  as a function of  $r$  for the three dimensional hard sphere fluid at a variety of densities as sketched in the figure.
2. Plots of  $\xi_{\text{rattle}}$  as a function of  $\rho$  for  $D=2$  (squares) and  $D=3$  (circles). Uncertainties correspond to standard deviations in this data as obtained from block averages. The triangles are experimental cage sizes for hard spheres as reported by [21]. Here we have normalized the experimental cage sizes by the bead diameter. Since our definition of  $\xi_{\text{rattle}}$  may be expected to be smaller than the cage size by a factor of 2, we divide the experimental data by 2 to ensure a proper comparison. The full line is the best fit to the cell model form  $\xi_{\text{rattle}} = \alpha \left[ \left( \frac{\rho_{\text{rcp}}}{\rho} \right)^{1/D} - 1 \right]$ , while the dotted line is a linear fit to lower density data as discussed in the text.
3. Cavity size,  $\xi_{\text{cavity}}$  plotted as a function of density. Main plot is for hard spheres and the inset is for disks. Uncertainties are standard deviations in the data. The dotted lines are best fits over the low density ranges as discussed in the text, while the full line is the best fit to the cell model form  $\xi_{\text{cavity}} = \alpha \left[ \left( \frac{\rho_{\text{rcp}}}{\rho} \right)^{1/D} - 1 \right]$ .
4. Data for the  $\xi_{\text{cross}}$  (squares) and  $\xi_{\text{ran}}$  (lines) for hard spheres [main plot] and disks [inset] as a function of density.

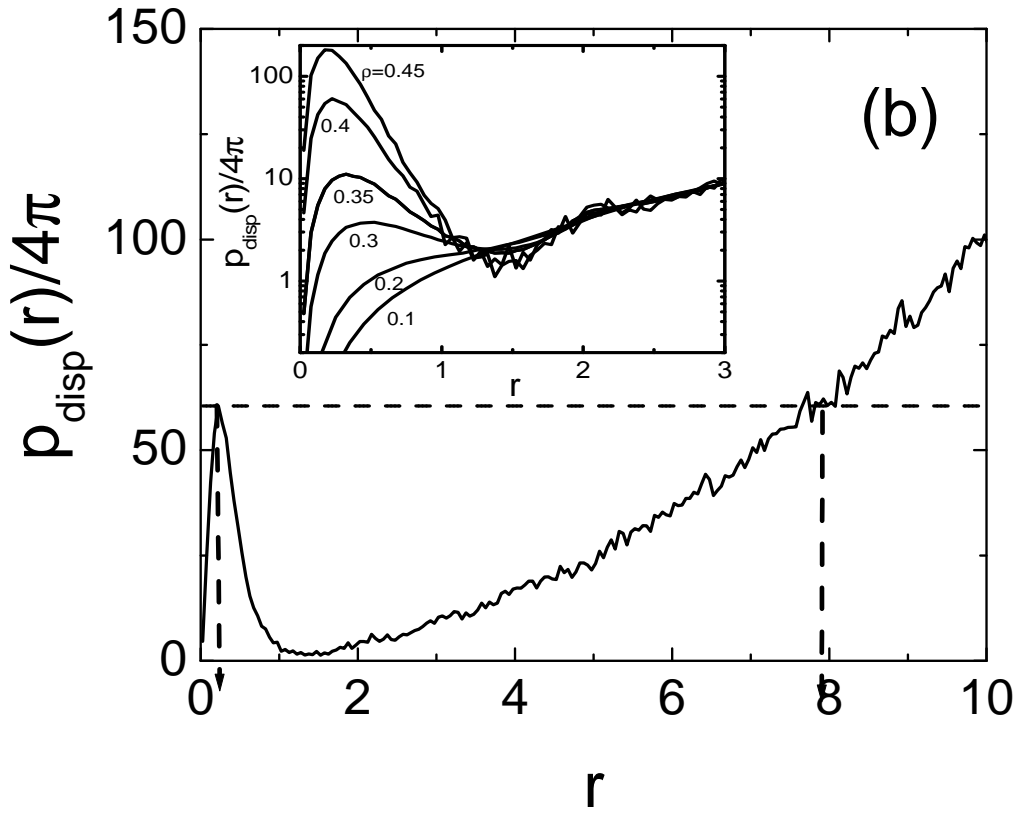
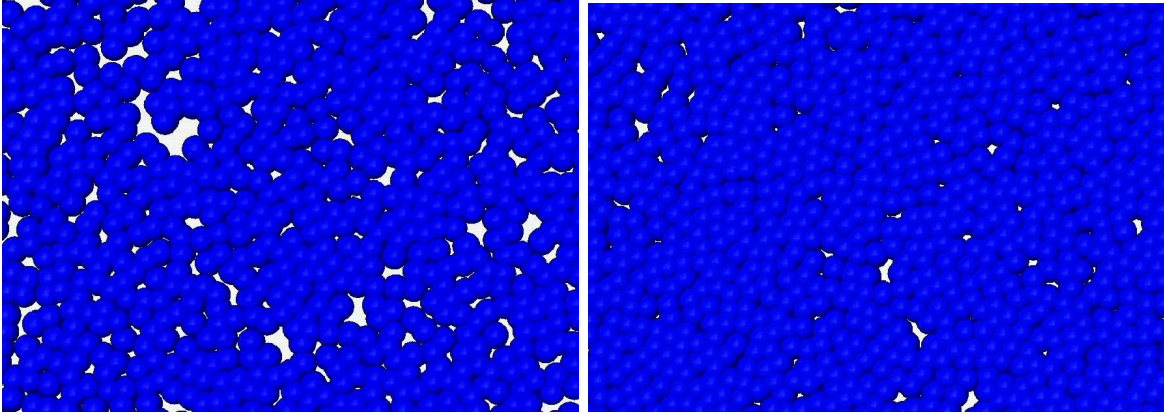


FIG. 1:

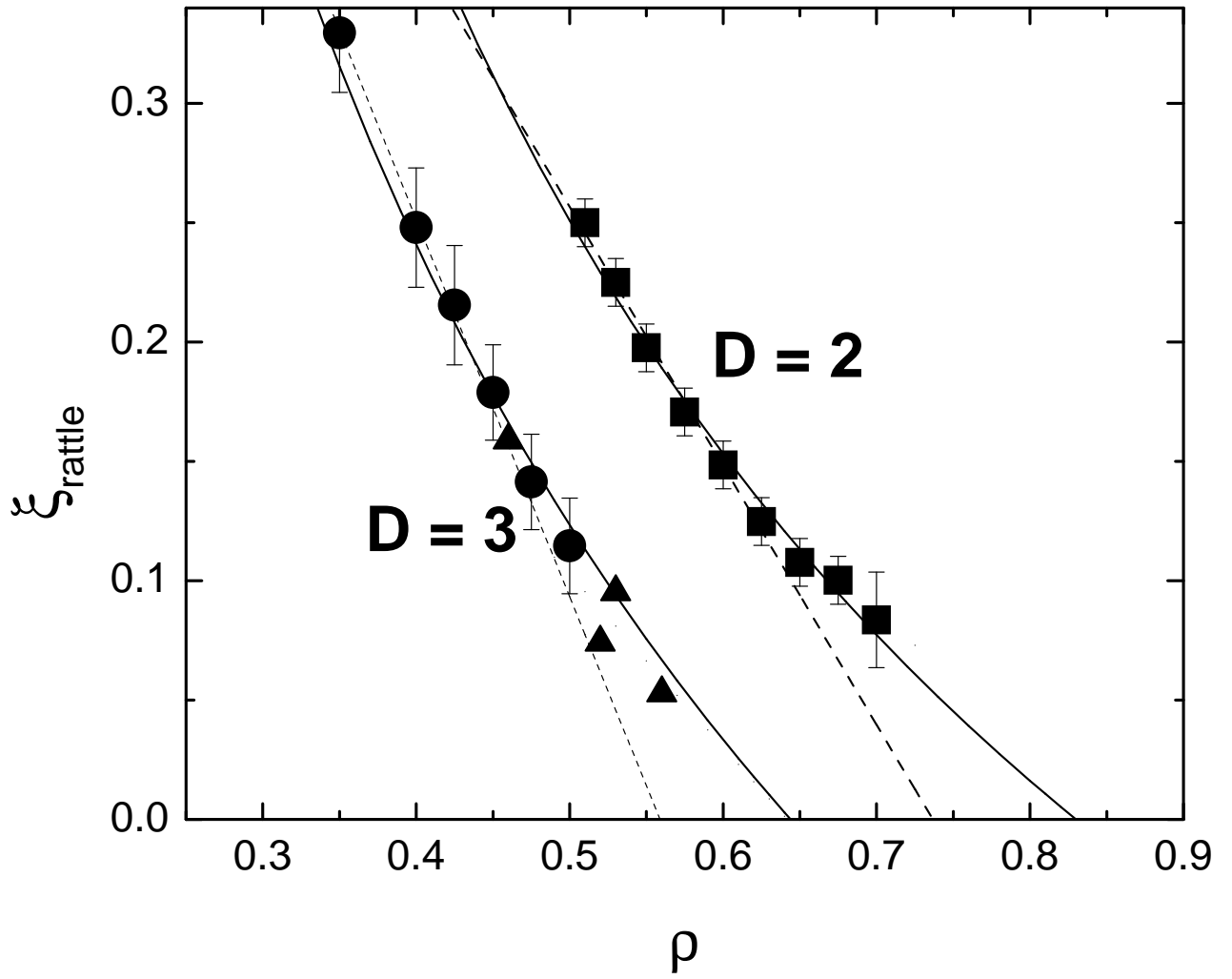


FIG. 2:

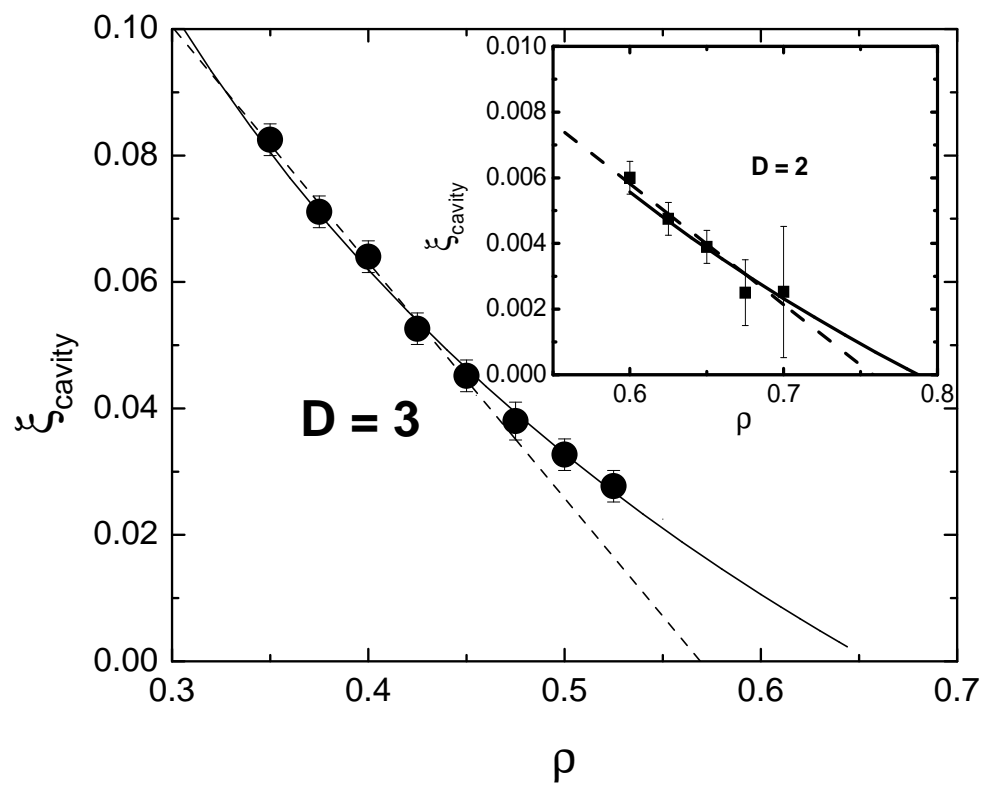


FIG. 3:

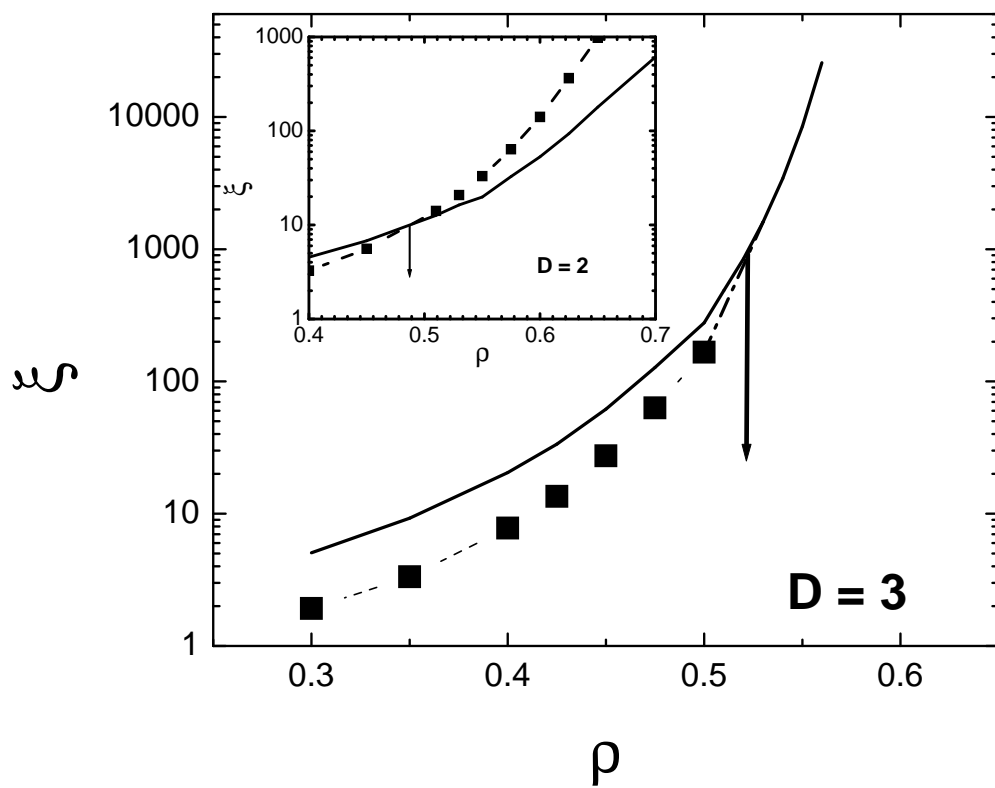


FIG. 4: